ELSEVIER

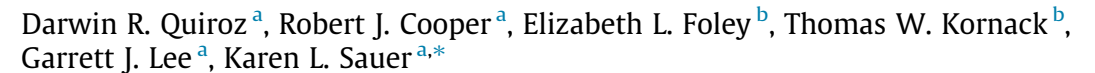
Contents lists available at ScienceDirect

# Journal of Magnetic Resonance

journal homepage: www.elsevier.com/locate/jmr



## Interleaved NQR detection using atomic magnetometers





<sup>&</sup>lt;sup>b</sup> Twinleaf LLC, Plainsboro 08536, NJ, USA



Article history:
Received 18 July 2022
Revised 29 August 2022
Accepted 30 August 2022
Available online 23 September 2022

Keywords:
Nuclear quadrupole resonance
Zero-field NMR
Double resonance
Magnetometer
Potassium chlorate
Ammonium nitrate

#### ABSTRACT

Interleaved Nuclear Quadrupole Resonance (NQR) detection was conducted on ammonium nitrate and potassium chlorate using two  $^{87}$ Rb magnetometers, where potassium chlorate is measured during the  $T_1$  limited recovery time of ammonium nitrate. The multi-pass magnetometers are rapidly matched to the NQR frequencies, 531 kHz and 423 kHz, with the use of a single tuning field. For ease of implementation, a double resonant tank circuit was used for excitation, but could be replaced by a broad-band transmitter. All work was done in an unshielded environment and compared to conventional coil detection. The two magnetometers were sensitive, base noise as low as  $2 \, {\rm fT/\sqrt{Hz}}$ , and were shown to reduce ambient noise through signal subtraction. When an excitation pulse was introduced, however, residual ringing increased the noise floor; mitigation techniques are discussed. The two detection techniques resulted in comparable Signal-to-Noise Ratio (SNR). Interleaved detection using the atomic magnetometers took half the time of conventional detection and provided localization of the explosives.

© 2022 Elsevier Inc. All rights reserved.

#### 1. Introduction

Ability to distinguish different chemical species has increased in demand over the decades, for both science and defense, and thus increased the need for non-invasive spectroscopic techniques such as NOR. In particular, zero-field nuclear magnetic resonance (NMR) or NQR spectroscopy is used to detect quadrupolar nuclei with nuclear spin I > 1/2. NQR frequencies are determined by the local electric-field gradient at the nucleus due to the surrounding electronic environment. Detection is conventionally done using a Faraday coil tuned to the NQR frequency and can be conducted nondestructively in powdered samples. This, coupled with a unique spectral signature [1], makes NQR attractive for a variety of applications, such as detection of explosives and narcotics [2-4], as well as pharmaceuticals [5-7], and to study magnetic properties of superconductors [8-10]. Yet, NQR detection is often limited by long  $T_1$  times, such as the  $T_1 = 17$  s for ammonium nitrate [11]. In addition, because of the unique and often widely spaced spectrum, conventional coil detection for multiple materials is done serially, where variations in electrical components for each NQR frequency [12,13] limit scalability.

In contrast, atomic magnetometers can be easily tuned to an NQR frequency by small adjustments to the field coils [14]. They

E-mail address: ksauer1@gmu.edu (K.L. Sauer).

also maintain a high sensitivity to ultra-low magnetic fields. Over recent years, sensitivities have rivaled superconducting quantum interference devices (SQUIDS) [15], without the need for cryogenics [16]. As a result, atomic magnetometers have been applied to biomagnetics [17–22], geomagnetics [23,24], search for axion and axion-like particles through the GNOME collaboration [25–28], and in particular, in the RF regime, for NMR [29–31], including NQR [32–35]. Furthermore, they are insusceptible to electric field noise and inductive coupling, often present in Faraday coil arrays; as a result, they provide an efficient method for RF interference mitigation when used as gradiometers [36,37].

Taking advantage of the easy tunability, atomic magnetometers allow for long relaxation times to be compensated for by using interleaved detection. Paired with broadband excitation [38], switching between frequencies becomes trivial. Using atomic magnetometers with multiple probe passes for increased sensitivity, we demonstrate the ability to cut in half the detection time of two nuclei using interleaved detection. The magnetometers are tuned by only adjusting the static tuning field  $B_0$ , matching the Larmor precession of the Rb atoms to the NQR frequency. Only the current applied to the tuning field of the magnetometer is used to match to the NQR frequency. By comparing the relative signals across two magnetometers, localization of explosives and sources of noise are distinguishable. For simplicity in demonstration, however, a doubly-tuned resonant circuit was designed and used for excitation. The following discussion will compare conventional coil

<sup>\*</sup> Corresponding author.

detection done sequentially to interleaved magnetometer detection. Common materials used in improvised explosives devices, ammonium nitrate and potassium chlorate, are detected in an unshielded environment with the RF coils in free space.

## 2. Experiment

To generate the NQR excitation pulses, a double-resonance tank circuit, described in Section 2.3, was constructed. For detection by atomic magnetometers, two separate magnetometers were placed symmetrically under the coil, see Fig. 1. All work was done using a spin-lock spin-echo sequence, shown in Fig. 2. The sequence timings were made to accommodate a time between refocusing pulses of  $2\tau \approx 2$  ms. Standard phase cycling techniques were used to mitigate ringing from the excitation pulse.

For convenience, the two (0.48 kg of KCLO $_3$  and 0.36 kg of NH $_4$ -NO $_3$ ) samples were temperature-controlled to lock in their resonance frequency [39],[40]. In addition, a sniffer coil, placed  $\sim$ 0.7 m away, was used to calibrate the RF fields.

## 2.1. Conventional NQR

Conventional coil detection used the same tank circuit for excitation as for detection. Moreover, a  $\pi$ -network was connected in series to the receiver for protection against the transmitted RF pulses [41]. Detection was done serially, as the receiver's  $\pi$ -network needed to be changed between samples.

#### 2.2. Atomic magnetometers

Two optically heated <sup>87</sup>Rb magnetometer sensors (Twinleaf LLC) replaced the receiver used for conventional coil detection, placed 1 cm below the bottom of each sample and 8 cm apart, that are optically heated to create an alkali vapor. The magnetometers are tuned using magnetic fields of less than 0.1 mT to adjust the <sup>87</sup>Rb atoms Larmor frequency to match the NQR frequency. A set of small field coils directly around each sensor and two larger field coils surrounding both sensors compensate for Earth's field, as well as tune and shim the magnetometers. The largest field coil, designed to be highly homogeneous [33], is used to change the resonance frequency as is shown in Fig. 1. In addition, an offset field of

0.85 G is applied during the RF pulse to detune the magnetometer from the frequency of the excitation pulse. This detuning field is inhomogeneous to temporarily shorten  $T_2^*$  to reduce ringing. Furthermore a diode ladder, shown in Fig. 3, serves to terminate the dissipating energy of the high-Q probe quickly after the RF pulse ends, again to reduce the ringing. The conventional coil detection does not have this diode ladder.

The Rb cells are optically pumped at the  $D_1$  line to polarize the atoms. The pump laser is modulated through the current of the tapered optical amplifier, but could be better controlled with an acousto-optic modulator. The signal is then acquired from a linearly-polarized and off-resonant probe beam orthogonal to the pump light direction. The beam passes back and forth through the cell more than 30 times, for increased sensitivity, before being detected by a balanced polarimeter.

#### 2.3. Design of the Double-tuned Resonance Circuit

A tank circuit was designed to resonate at two distinct frequencies  $f_L$  and  $f_H$ , implementing only reactive elements to minimize resistance and power loss delivery to the probe. The circuit is comprised of four main components: the sample coil that hosts the samples, a trap network to create a pole at frequency  $f_{Trap}$ , a matching component made to impedance match the circuit to a 50  $\Omega$  load, and a series coupling capacitor that will be used to shift the two frequencies to the target. The basic design is based on that of [42]; by considering the admittance Y = 1/Z of the circuit given in Fig. 3,

$$\Re(Y_{\textit{Match}}) + \Re(Y_{\textit{Load}}) = 1/50\Omega, \tag{1}$$

$$\mathfrak{I}(Y_{Match}) = -\mathfrak{I}(Y_{Load}),\tag{2}$$

where  $Y_{Load}$  is the admittance of the load,  $Y_{Match}$  is the admittance of the matching element. Eqs. (1) and (2) must be satisfied at  $f_L$  and  $f_H$  to provide a unique solution for the four unknowns  $L_1, L_M, C_1, C_2$  of the circuit. Initial design proceeded with assumption of idealized components. Numerical methods were used afterwards to find the final values, taking into account resistances and using Eqs. (1) and (2).

In the limit that the solenoid resistance  $R_s$  is the only significant resistance, Eq. (1) becomes

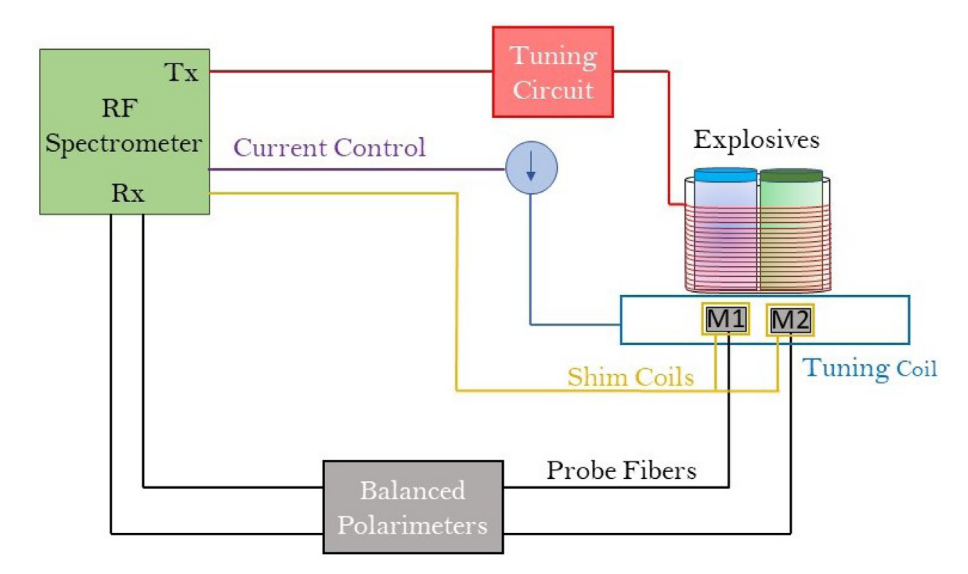


**Fig. 1.** Experimental setup used for atomic magnetometer detection. The explosive samples are placed in the excitation coil to produce the RF field. The magnetometers M1 and M2 are then tuned to the NQR frequency using the shim and tuning coils and optical signals acquired using a balanced polarimeter; the fiber-coupled lasers are not shown

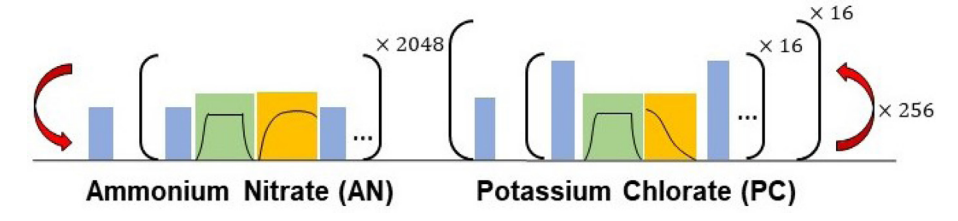
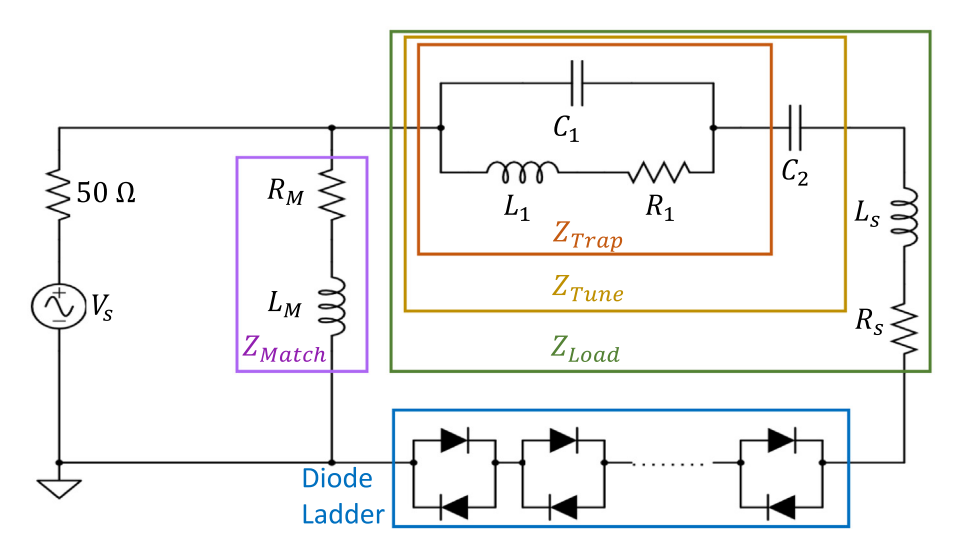


Fig. 2. Spin-Lock Spin-Echo (SLSE) sequences, interleaved between ammonium nitrate and potassium chlorate. The radio-frequency pulses used to excite and refocus the nuclei are shaded in blue; an offset field was applied during this time. Light pulses that pump the sensors are defined by the green shading, and are adiabatically ramped up and down to avoid perturbations before acquisition of the NQR signal, shaded in yellow. Interleaved sequencing was repeated over 256 times, with no wait times between different sequences.



**Fig. 3.** The tuning network is defined by the coupling capacitor ( $C_2$ ) and trap elements ( $L_1$  and  $C_1$ ) with an overall impedance  $Z_{Tune}$ . The circuit's load would be the equivalent series connection between the sample coil and tuning network with impedance  $Z_{Tune} + i\omega L_s + R_s$ , where the resistance of the diode ladder is included into  $R_s$ . The total impedance of the circuit is then the parallel combination between the matching network and load  $Z_{Match}||Z_{Load}|$ .

$$50\Omega = (R_s^2 + X_{land}^2)/R_s,$$
 (3)

where  $X_{Load}$  is the reactance of the load, as per Fig. 3. Expanding  $X_{Load}$  in terms of its circuit elements, Eq. (3) can be rewritten as

$$X_{\text{Load}} = X_{\text{Tune}} + \omega L_{\text{s}} = \pm \sqrt{(50\Omega)R_{\text{s}} - R_{\text{s}}^2} \ll 50\Omega, \tag{4} \label{eq:Load}$$

where  $X_{Tune} = X_{Trap} - 1/\omega C_2$  is the equivalent reactance of the trap and tuning capacitor shown in Fig. 3. Eq. (4) is to be satisfied at the two frequencies, using the three components of the tuning network. An additional equation is obtained by the LC trap circuit, creating a pole at  $f_{Trap}$  between the two frequencies,

$$2\pi f_{Trap} = \frac{1}{\sqrt{L_1 C_1}};\tag{5}$$

design of  $f_{Trap} = (f_L + f_H)/2$  is a natural choice. Fig. 4a shows the graphical solution to Eq. (4) in the limit of negligible  $R_s$ , refined experimentally. The reactance measured from the tuning network and  $L_s$  from Fig. 4a, show that Eq. (4) is satisfied at target frequencies  $f_s$  and  $f_{tr}$ .

To then impedance match the circuit to 50  $\Omega$ , Eq. (2) becomes

$$-X_{Match} = 50\Omega(R_s/X_{Load}), (6)$$

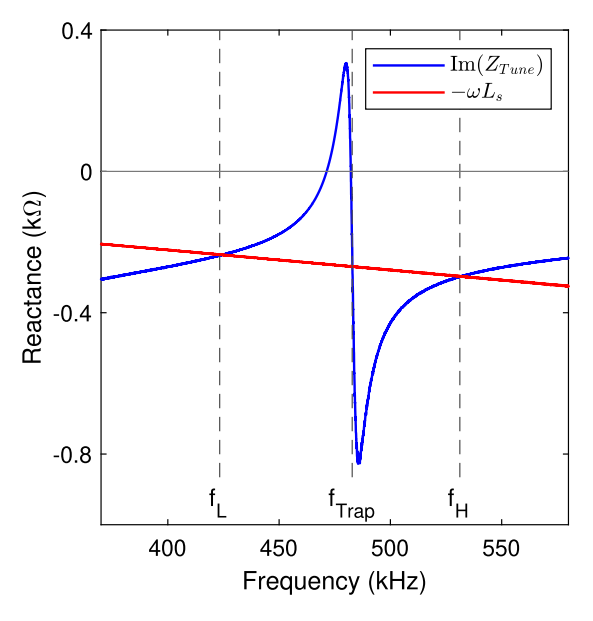
using Eq. (3). By choosing to use a matching inductor, as opposed to a matching capacitor,  $X_{Load}$  is fixed as negative. Furthermore, to satisfy Eq. (6), the load reactance must be adjusted so that

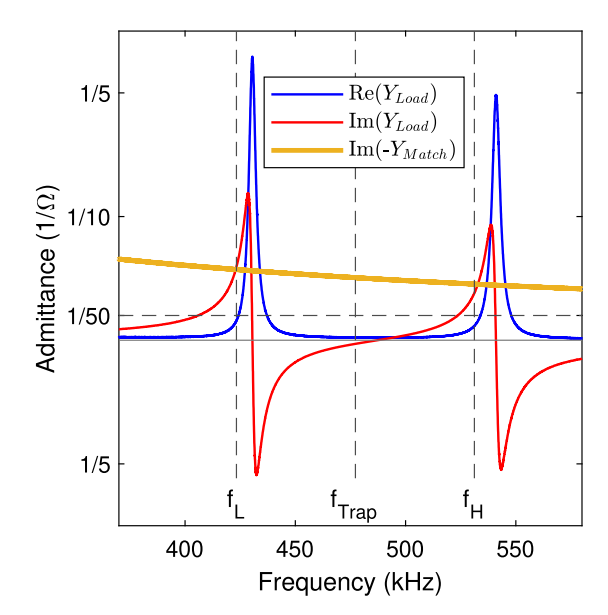
$$\frac{X_{Load}(\omega_L)}{X_{Load}(\omega_H)} = \frac{f_H}{f_L}.$$
 (7)

The pole produced by Eq. 5 provides a condition for double matching, resulting in two resonant peaks shown in red in Fig. 4b. Circuit resonances are shifted upwards to meet requirements of Eq. (4) with finite  $R_{\rm s}$ , and to ensure positive admittance required by a matching inductor. The matching inductor can then be chosen to roughly match Eq. (6) for the two resonances. When including finite resistances of the inductors, fine tuning of all elements are made to fit Eq. (1) and (2), as shown in Fig. 4b. The resulting impedance matching is shown in Fig. 5a. The RF field strengths used for NH<sub>4</sub>-NO<sub>3</sub> in both detection methods are given in Fig. 5b, where fields > 0.1 mT were achieved when the circuit is powered by a 1 kW amplifier. The field strength of the excitation and refocusing pulses used for magnetometer detection were increased to account for the shorter pulse decay.

## 3. Results

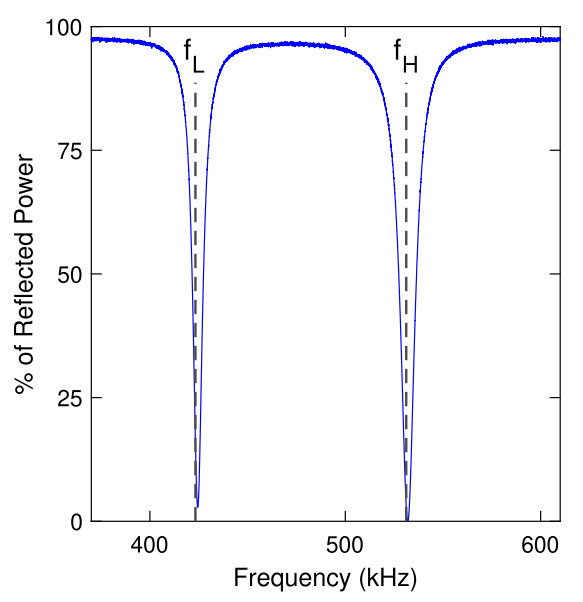
Signal-to-noise ratio (SNR) for both detection techniques were very similar for ammonium nitrate (AN) and potassium chlorate (PC) as shown in Fig. 6. The detection by the magnetometers, however, took half the time as conventional, due to interleaving; where time lost between changing receiver circuits for the NQR experiments are excluded. Excitation parameters and data processing, were the same for both techniques. Matched filtering was applied to the spectra of PC, both to the echo train and individual echoes to improve the SNR [40]. From Figs. 6b and d, the low SNR is due to the short acquire time limited by the material. For PC, the echo train decay time is 26 ms, and the echo is Gaussian in time with

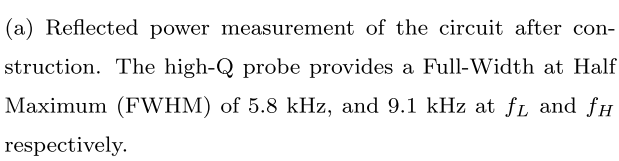


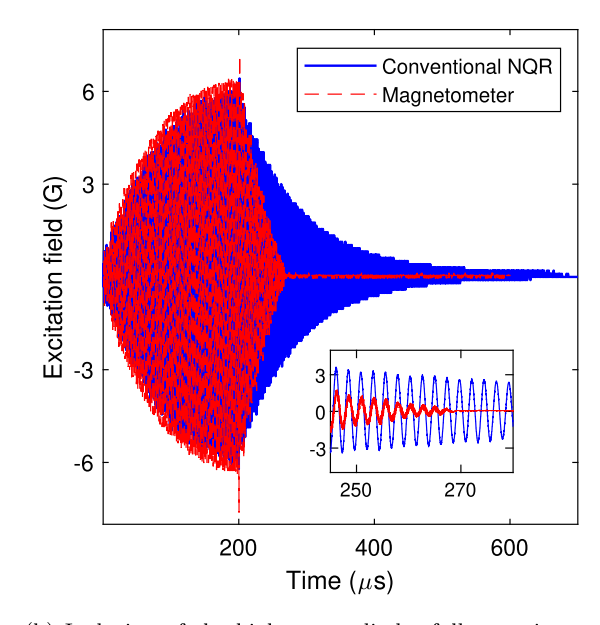


- (a) Experimentally measured reactance of the probe  $\omega L_s$  and tuning network  $X_{tune}$ . Intersecting frequencies correspond to the constraints set by Eq. (4), and pole produced at  $f_{Trap}$ .
- (b) Experimentally measured admittance of both the load and matching networks. Intersection frequencies correspond closely to the constraints set by Eq. (1) and (2).

**Fig. 4.** The double resonant tank circuit is shown in Fig. 3, to impedance match at frequencies  $f_L = 423.3$  kHz and  $f_H = 531.2$  kHz. The LC trap formed by  $Z_{Trap}$  creates a pole at  $f_{Trap} = 483.3$  kHz to achieve double resonance. The general procedure to satisfy Eq. (1) and (2) is shown in Fig. 4a and b.







(b) Inclusion of the high-power diodes fully terminates the dissipating magnetic energy in  $\sim 70~\mu s$  after the RF pulse ends, while the natural decaying signal continues for well over 600  $\mu s$ .

Fig. 5. Reflected power after circuit construction is shown in Fig. 5a and the RF pulses produced for NH<sub>4</sub>NO<sub>3</sub> across both setups are shown in Fig. 5b.

a half-width-half-maximum (HWHM) linewidth of 0.3 ms. In contrast, AN has an echo train decay time of 4 s with a HWHM of 1 ms. The total effective acquire time was kept consistent across both detection methods at 524 s and 19.7 s for AN and PC respectively, and includes the echo window, the number of echoes and sequence repetitions.

Measured values of the signals, for conventional and magnetometer detection, were close to estimates based on modelling with bound surface currents, as shown in Table 1. The fields produced by PC are expected to be larger than AN due to the sample masses. In addition, lower field strengths are expected from conventional coil detection because the physical space of the bottle

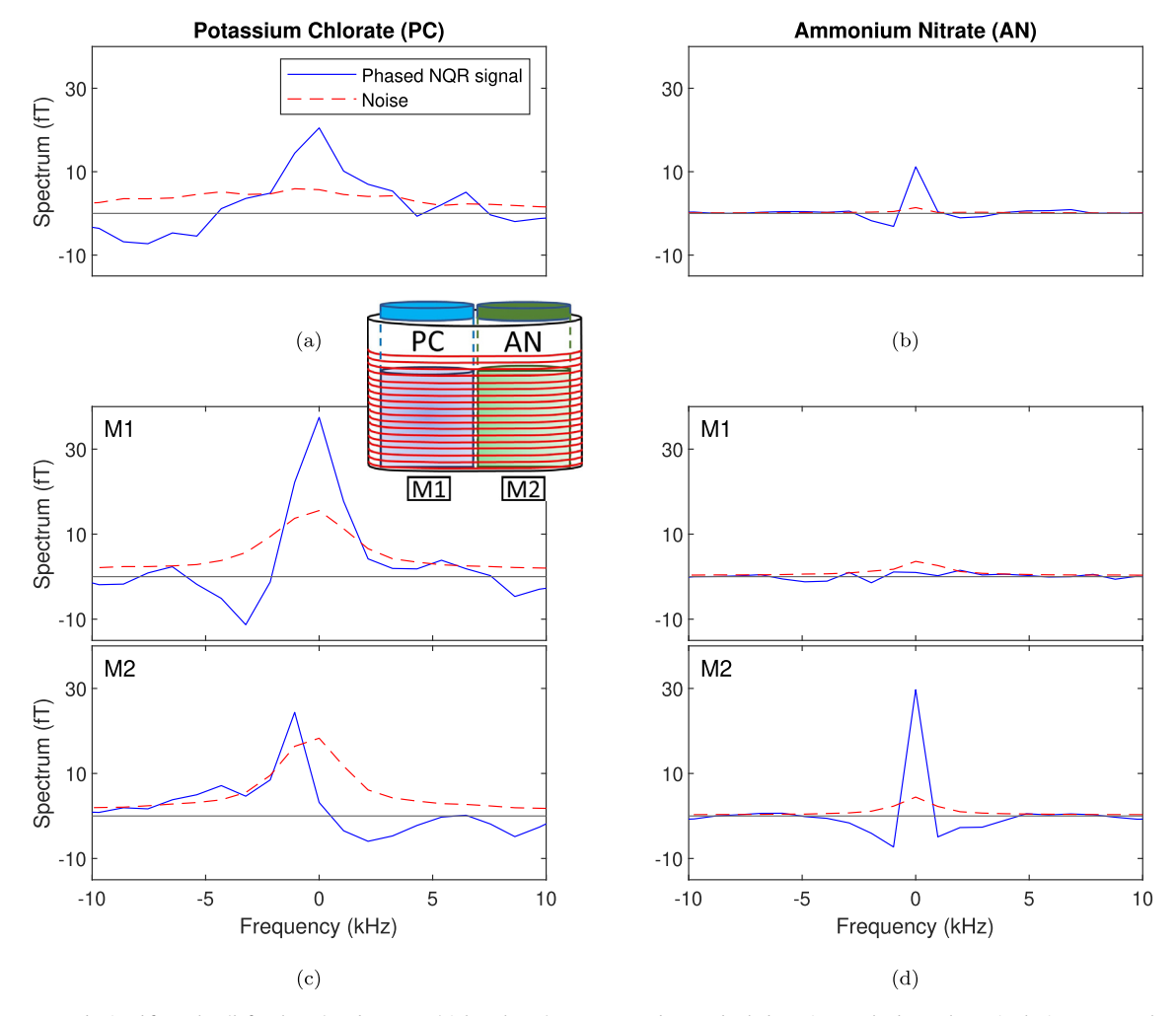


**Fig. 6.** The spectrum obtained for  $KClO_3$  (left column) and  $NH_4NO_3$  (right column) are compared across both detection methods. As shown in the inset, a sample of PC is above Magnetometer 1 (M1) and AN above Magnetometer 2 (M2). Spectra for AN are centered at 423.3 kHz, while the spectra of PC are centered at 531.2 kHz. The spectrum of both explosives using conventional coil detection are shown in Figs. 6a and b, while the spectra obtained using interleaved magnetometer detection are shown in Figs. 6c and d. Localization of the two explosives is obtained by comparing signals from the two magnetometers M1 (middle row) and .M2 (bottom row).

Table 1
Measured and predicted field strengths for both materials and methods.

	Conventional		Quantum Magnetometer	
	Predicted (fT)	Measured (fT)	Predicted (fT)	Measured (fT)
AN	14	$11.2\pm1.4$	31	$30\pm 4$
PC	22	$21 \pm 6$	48	$36\pm15$

only partially filled the detector coil. Spectra obtained for both detection methods are shown in Fig. 6. The spectra for PC across both methods are broader due to its linewidth.

Ambient room noise is consistent with  ${\sim}30~\text{fT}/\sqrt{\text{Hz}}$  for conventional and  ${\sim}80~\text{fT}/\sqrt{\text{Hz}}$  for magnetometer detection. The difference suggests equipment associated with the magnetometer contributes more environmental noise, which in principle could be eliminated with careful shielding of the equipment. From Fig. 7a, subtraction reduces the noise by a factor of 5 when the RF pulse is not activated. Furthermore, a baseline sensitivity of 2 fT/ $\sqrt{\text{Hz}}$  is measured for one sensor when the atoms are not pumped, giving the lower limit to the sensitivity. With the RF pulse, and the accompanying offset field pulse, the noise is not common-mode as shown in Fig. 7b, and is not coherent with the RF pulse as shown in Fig. 7c. The lack of coherence with the offset pulse and between sensors suggests the noise arises from spin dynamics occurring

from the combination of the inhomogeneous offset pulse and the light pulse. When the pulse is not aligned with the static field, a transverse fictitious magnetic field is created, resulting in noise.

## 4. Conclusion

A method for interleaved NQR detection using atomic magnetometers was demonstrated using the  $^{14}$ N line of AN and  $^{39}$ K line of PC. This technique provided a means of utilizing the dead time present from the long  $T_1$  time of AN and to a lesser extent, the  $T_1$  of PC. Since changing the sensor's frequency only required changing the current applied to the magnetometer's tuning coil, additional resonance frequencies could be easily accommodated, providing a scalable solution. Furthermore, the location of the explosives were determined by using a pair of magnetometers. For comparison, conventional coil detection was conducted

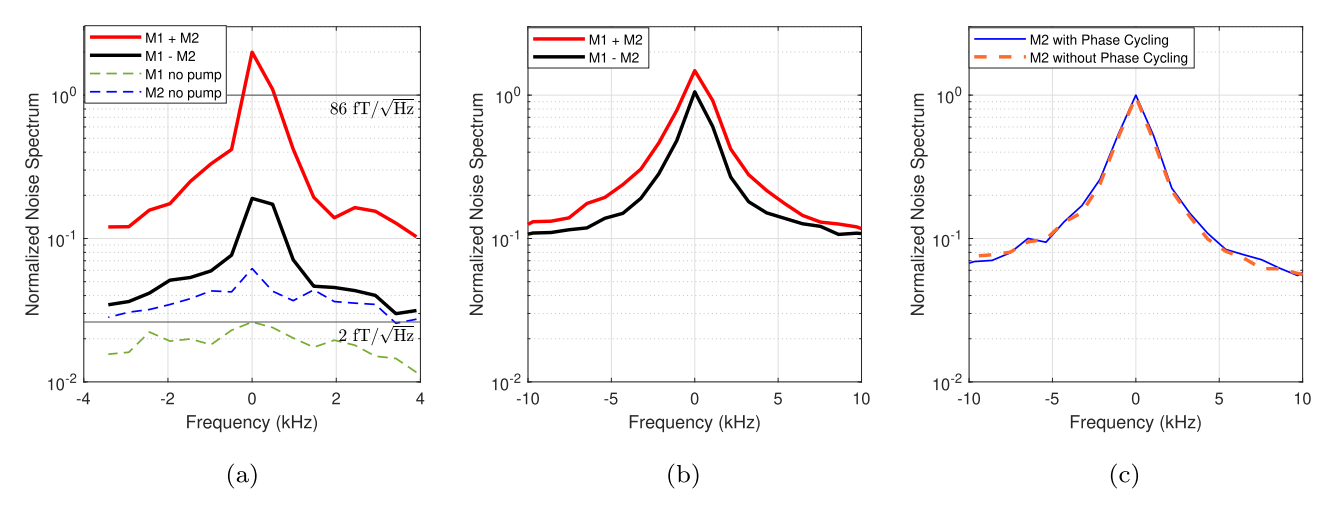


Fig. 7. The noise spectra for AN magnetometer detection are shown, all spectra are normalized with respect to the noise of M2, shown on the far right. (a) When no RF pulse is used, common mode noise is effectively subtracted. The fundamental noise limit across M1 and M2 are shown in dashed lines when the light pulse is also removed. (b) With the RF pulse active, common-mode noise is not effectively subtracted out. (c) Furthermore, phase cycling, standardly used to reduce noise, is also ineffective. Details discussed in the text.

sequentially for both samples, because of the receiver tuning. Both techniques showed similar SNR, but with the magnetometers only taking half the time from detection interleaving.

Although the demonstration of interleaving was successful, the magnetometers were susceptible to noise generated with the combination of the excitation and pump-light pulses. When the RF pulse was inactive, subtraction of common-mode noise between the two unshielded sensors was shown to improve the sensitivity by a factor of 5. In the presence of an RF pulse however, this subtraction was no longer effective; the pump-light pulse was not strong enough to remove the effect of the RF pulse. Ringing within the excitation circuit, for instance from magneto or piezo electric ringing, was also ruled out, as noise coming through the excitation coil would be common to both sensors. While a detuning field partially mitigated the effects of the RF pulse, it also misaligned the static field from the pump light, an effect exacerbated by instrumental lag time. Therefore, the resulting noise was no longer coherent with the RF pulse, so standard phase cycling techniques were ineffective.

Future work will explore other ringing mitigation techniques such as spin-damping through active feedback [43], one-sided excitation coils [32], and improved timing and alignment between pump and tuning fields to avoid triggering fictitious magnetic fields [14]. If these techniques are successful, such that noise can be brought down to the base noise of the sensors,  $2 \text{ fT}\sqrt{\text{Hz}}$ , sensitivity would improve to be an order of magnitude better than conventional coil detection. Coupled with the ability to rapidly tune, and therefore interleave detection between different materials, potential benefits of developing and using atomic magnetometers is clear.

#### **Declaration of Competing Interest**

The authors declare that they have no known competing financial interests or personal relationships that could have appeared to influence the work reported in this paper.

#### Acknowledgements

This work was supported, in part, by the National Science Foundation (award 171118).

#### References

- [1] A. Garroway, M. Buess, J. Miller, B. Suits, A. Hibbs, G. Barrall, R. Matthews, L. Burnett, Remote sensing by nuclear quadrupole resonance, IEEE Trans. Geosci. Remote Sens. 39 (6) (2001) 1108–1118, https://doi.org/10.1109/36.927420.
- [2] J.B. Miller, G.A. Barrall, Explosives Detection with Nuclear Quadrupole Resonance: An emerging technology will help to uncover land mines and terrorist bombs, Am. Sci. 93 (1) (2005) 50–57.
- [3] J.B. Miller, Nuclear quadrupole resonance detection of explosives: an overview, in: R.S. Harmon, J.H.H. Jr., J.T. Broach (Eds.), Detection and Sensing of Mines, Explosive Objects, and Obscured Targets XVI, Vol. 8017, International Society for Optics and Photonics, SPIE, 2011, pp. 404 410. doi:10.1117/12.887213.
- [4] J. Yinon, Counterterrorist detection techniques of explosives, Elsevier, 2011.
- [5] Z. Trontelj, J. Pirnat, V. Jazbinšek, J. Lužnik, S. Srcic, Z. Lavric, S. Beguš, T. Apih, V. Žagar, J. Seliger, Nuclear Quadrupole Resonance (NQR)—A Useful Spectroscopic Tool in Pharmacy for the Study of Polymorphism, Crystals 10 (6). doi:10.3390/cryst10060450.
- [6] T. Apih, V. Žagar, J. Seliger, NMR and NQR study of polymorphism in carbamazepine, Solid State Nucl. Magn. Reson. 107 (2020) 101653, https:// doi.org/10.1016/j.ssnmr.2020.101653.
- [7] J. Barras, D. Murnane, K. Althoefer, S. Assi, M.D. Rowe, I.J.F. Poplett, G. Kyriakidou, J.A.S. Smith, Nitrogen-14 Nuclear Quadrupole Resonance Spectroscopy: A Promising Analytical Methodology for Medicines Authentication and Counterfeit Antimalarial Analysis, Anal. Chem. 85 (2013) 2746, https://doi.org/10.1021/ac303267v.
- [8] K. Ishida, Y. Kitaoka, N. Ogata, T. Kamino, K. Asayama, J.R. Cooper, N. Athanassopoulou, Cu NMR and NQR Studies of Impurities-Doped  $YBa_2(Cu_{1-x}M_x)_3O_7$  (M=Zn and Ni), J. Phys. Soc. Jpn. 62 (8) (1993) 2803–2818, https://doi.org/10.1143/JPSJ.62.2803.
- [9] C.G. Wang, Y. Honjo, L.X. Zhao, G.F. Chen, K. Matano, R. Zhou, G. qing Zheng, Landau diamagnetism and Weyl-fermion excitations in TaAs revealed by <sup>75</sup>As NMR and NQR, Phys. Rev. B 101 (2020) 241110. doi:10.1103/ PhysRevB.101.241110.
- [10] C. Mu, Q. Yin, Z. Tu, C. Gong, H. Lei, Z. Li, J. Luo, S-Wave Superconductivity in Kagome Metal CsV<sub>3</sub>Sb<sub>5</sub> Revealed by <sup>121/123</sup>Sb NQR and <sup>51</sup>V NMR Measurements, Chin. Phys. Lett. 38 (7) (2021) 077402, https://doi.org/ 10.1088/0256-307x/38/7/077402.
- [11] J. Barras, M.J. Gaskell, N. Hunt, R.I. Jenkinson, K.R. Mann, D.A.G. Pedder, G.N. Shilstone, J.A.S. Smith, Detection of ammonium nitrate inside vehicles by nuclear quadrupole resonance, Appl. Magn. Reson. 25 (2004) 411, https://doi.org/10.1007/BF03166538.
- [12] T.N. Rudakov, B. Rameev, G. Mozzhukhin, J. Barras, Further Improvement of NQR Technique for Detection of Illicit Substances, in: T. Apih (Ed.), Magnetic Resonance Detection of Explosives and Illicit Materials, Springer, Netherlands, Dordrecht, 2014, pp. 3–17.
- [13] C. Monea, G.V. Iana, S. Ionita, L.M. Ionescu, S.A. Zaharia, S. Ilie, N. Bizon, An optimized NQR spectrometer for detection of prohibited substances, Measurement 151 (2020) 107158, https://doi.org/10.1016/j.measurement.2019.107158.
- [14] I.M. Savukov, S.J. Seltzer, M.V. Romalis, K.L. Sauer, Tunable Atomic Magnetometer for Detection of Radio-Frequency Magnetic Fields, Phys. Rev. Lett. 95 (2005) 063004, https://doi.org/10.1103/PhysRevLett.95.063004.
- [15] M. Schmelz, V. Zakosarenko, A. Chwala, T. Schönau, R. Stolz, S. Anders, S. Linzen, H.-G. Meyer, Thin-Film-Based Ultralow Noise SQUID Magnetometer, IEEE Trans. Appl. Supercond. 26 (5) (2016) 1–5, https://doi.org/10.1109/TASC 2016 2530699

- [16] I.K. Kominis, T.W. Kornack, J.C. Allred, M.V. Romalis, A subfemtotesla multichannel atomic magnetometer, Nature 422 (6932) (2003) 596–599, https://doi.org/10.1038/nature01484.
- [17] T.H. Sander, J. Preusser, R. Mhaskar, J. Kitching, L. Trahms, S. Knappe, Magnetoencephalography with a chip-scale atomic magnetometer, Biomed. Opt. Express 3 (5) (2012) 981–990, https://doi.org/10.1364/BOE.3.000981.
- [18] A.P. Colombo, T.R. Carter, A. Borna, Y.-Y. Jau, C.N. Johnson, A.L. Dagel, P.D.D. Schwindt, Four-channel optically pumped atomic magnetometer for magnetoencephalography, Opt. Express 24 (14) (2016) 15403–15416, https://doi.org/10.1364/OE.24.015403.
- [19] K. Kim, S. Begus, H. Xia, S.-K. Lee, V. Jazbinsek, Z. Trontelj, M.V. Romalis, Multichannel atomic magnetometer for magnetoencephalography: A configuration study, NeuroImage 89 (2014) 143–151, https://doi.org/10.1016/j. neuroimage.2013.10.040.
- [20] E. Labyt, M.-C. Corsi, W. Fourcault, A. Palacios Laloy, F. Bertrand, F. Lenouvel, G. Cauffet, M. Le Prado, F. Berger, S. Morales, Magnetoencephalography With Optically Pumped <sup>4</sup>He Magnetometers at Ambient Temperature, IEEE Transactions on Medical Imaging 38 (1) (2019) 90–98. doi:10.1109/TMI.2018.2856367.
- [21] J. Zhang, K. Liu, J. Zhang, Z. Wang, J. Shang, Magnetocardiography Measurements by Microfabricated Atomic Magnetometer With a 3-D Spherical Alkali Vapor Cell, IEEE Trans. Instrum. Meas. 70 (2021) 1–7, https://doi.org/10.1109/TIM.2021.3120375.
- [22] E. Botó, S.S. Meyer, V. Shah, O. Alem, S. Knappe, P. Kruger, T.M. Fromhold, M. Lim, P.M. Glover, P.G. Morris, R. Bowtell, G.R. Barnes, M.J. Brookes, A new generation of magnetoencephalography: Room temperature measurements using optically-pumped magnetometers, NeuroImage 149 (2017) 404–414, https://doi.org/10.1016/j.neuroimage.2017.01.034.
- [23] H.B. Dang, A.C. Maloof, M.V. Romalis, Ultrahigh sensitivity magnetic field and magnetization measurements with an atomic magnetometer, Appl. Phys. Lett. 97 (15) (2010) 151110, https://doi.org/10.1063/1.3491215.
- [24] M.J. Usher, W.F. Stuart, S.H. Hall, A self-oscillating rubidium vapour magnetometer for geomagnetic measurements, J. Sci. Instrum. 41 (9) (1964) 544–547, https://doi.org/10.1088/0950-7671/41/9/305.
- [25] S. Pustelny, D.F. Jackson Kimball, C. Pankow, M.P. Ledbetter, P. Wlodarczyk, P. Wcislo, M. Pospelov, J.R. Smith, J. Read, W. Gawlik, D. Budker, The Global Network of Optical Magnetometers for Exotic physics (GNOME): A novel scheme to search for physics beyond the Standard Model, Annalen der Physik 525 (8–9) (2013) 659–670. doi:10.1002/andp.201300061.
- [26] P. Wlodarczyk, S. Pustelny, D. Budker, M. Lipinski, Multi-channel data acquisition system with absolute time synchronization, Nucl. Instrum. Methods Phys. Res., Sect. A 763 (2014) 150–154, https://doi.org/10.1016/j. nima.2014.05.126.
- [27] J. Lee, A. Almasi, M. Romalis, Improved Limits on Spin-Mass Interactions, Phys. Rev. Lett. 120 (2018) 161801, https://doi.org/10.1103/ PhysRevLett.120.161801.
- [28] S. Afach, B.C. Buchler, D. Budker, C. Dailey, A. Derevianko, V. Dumont, N.L. Figueroa, I. Gerhardt, Z.D. Grujic, H. Guo, C. Hao, P.S. Hamilton, M. Hedges, D.F. Jackson Kimball, D. Kim, S. Khamis, T. Kornack, V. Lebedev, Z.-T. Lu, H. Masia-Roig, M. Monroy, M. Padniuk, C.A. Palm, S.Y. Park, K.V. Paul, A. Penaflor, X. Peng, M. Pospelov, R. Preston, S. Pustelny, T. Scholtes, P.C. Segura, Y.K. Semertzidis, D. Sheng, Y.C. Shin, J.A. Smiga, J.E. Stalnaker, I. Sulai, D. Tandon, T. Wang, A. Weis, A. Wickenbrock, T. Wilson, T. Wu, D. Wurm, W. Xiao, Y. Yang, D. Yu, J. Zhang, Search for topological defect dark matter with a global network

- of optical magnetometers, Nat. Phys. 17 (2021) 1396–1401, https://doi.org/10.1038/s41567-021-01393-v.
- [29] I.M. Savukov, S.J. Seltzer, M.V. Romalis, Detection of NMR signals with a radio-frequency atomic magnetometer, J. Magn. Reson. 185 (2007) 214–220, https://doi.org/10.1016/j.jmr.2006.12.012.
- [30] I. Savukov, Y.J. Kim, G. Schultz, Detection of ultra-low field NMR signal with a commercial QuSpin single-beam atomic magnetometer, J. Magn. Reson. 317 (2020) 106780, https://doi.org/10.1016/j.jmr.2020.106780.
- [31] S. Xu, V.V. Yashchuk, M.H. Donaldson, S.M. Rochester, D. Budker, A. Pines, Magnetic resonance imaging with an optical atomic magnetometer, Proc. Nat. Acad. Sci. 103 (34) (2006) 12668–12671, https://doi.org/10.1073/pnas.0605396103.
- [32] S.-K. Lee, K.L. Sauer, S.J. Seltzer, O. Alem, M.V. Romalis, Subfemtotesla radio-frequency atomic magnetometer for detection of nuclear quadrupole resonance, Appl. Phys. Lett. 89 (21) (2006) 214106, https://doi.org/10.1063/1.2390643
- [33] R.J. Cooper, D.W. Prescott, P. Matz, K.L. Sauer, N. Dural, M.V. Romalis, E.L. Foley, T.W. Kornack, M.C. Monti, J.K. Okamitsu, Atomic Magnetometer Multisensor Array for RF Interference Mitigation and Unshielded Detection of Nuclear Quadrupole Resonance, Physical Review Applied 6 (2016) 064014.
- [34] M.C. Monti, D.A. Alexson, J.K. Okamitsu, NQR detection of explosive simulants using RF atomic magnetometers, in: S.S. Bishop, J.C. Isaacs (Eds.), Detection and Sensing of Mines, Explosive Objects, and Obscured Targets XXI, Vol. 9823, International Society for Optics and Photonics, SPIE, 2016, pp. 277 – 284. doi:10.1117/12.2224053.
- [35] M.W. Malone, G.A. Barrall, M.A. Espy, M.C. Monti, D.A. Alexson, J.K. Okamitsu, Polarization enhanced Nuclear Quadrupole Resonance with an atomic magnetometer, in: S.S. Bishop, J.C. Isaacs (Eds.), Detection and Sensing of Mines, Explosive Objects, and Obscured Targets XXI, Vol. 9823, International Society for Optics and Photonics, SPIE, 2016, pp. 285 – 291. doi:10.1117/ 12.2224070
- [36] D.A. Keder, D.W. Prescott, A.W. Conovaloff, K.L. Sauer, An unshielded radio-frequency atomic magnetometer with sub-femtoTesla sensitivity, AlP Advances 4 (12) (2014) 127159, https://doi.org/10.1063/1.4905449.
- [37] R.J. Cooper, D.W. Prescott, G.J. Lee, K.L. Sauer, RF atomic magnetometer array with over 40dB interference suppression using electron spin resonance, J. Magn. Reson. 296 (2018) 36–46, https://doi.org/10.1016/j.jmr.2018.08.007.
- [38] S. Mandal, Y.-Q. Song, Two-dimensional NQR using ultra-broadband electronics, J. Magn. Reson. 240 (2014) 16–23, https://doi.org/10.1016/j. jmr.2014.01.001.
- [39] D. Prescott, Nuclear Quadrupole Spin Dynamics: How Weak RF Pulses and Double Resonance Cross-Relaxation Contribute to Explosives Detection, Ph.D. thesis, George Mason University (2010).
- [40] K.E. Nixon, K.L. Sauer, Pulsed Spin-Locking of Spin-3/2 Nuclei: <sup>39</sup>K-NQR of Potassium Chlorate, J. Magn. Reson. 335 (2022) 107145, https://doi.org/ 10.1016/j.jmr.2022.107145.
- [41] E. Fukushima, S.B.W. Roeder, Experimental Pulse NMR A Nuts and Bolts Approach, Addison-Wesley, 1981.
- [42] M. Schnall, V. Harihara Subramanian, J. Leigh, B. Chance, A New Double-Tuned Probe For Concurrent <sup>1</sup>H and <sup>31</sup>P NMR, Journal of Magnetic Resonance (1969) 65 (1) (1985) 122–129, https://doi.org/10.1016/0022-2364(85)90380-4.
- [43] O. Alem, K.L. Sauer, M.V. Romalis, Spin damping in an RF atomic magnetometer, Phys. Rev. A 87 (2013) 013413, https://doi.org/10.1103/ PhysRevA.87.013413.